Crystal growth and physical characterization of bismaleato lead (IV) grown in silica gel

V Mahalakshmi, A Lincy, J Thomas and K V Saban*

Smart Materials Analytic Research and Technology (SMART), St. Berchmans College, Changanassery 686101, Kerala, India

*Corresponding author. Tel: +91 9847390370, Fax: +91 4812401472, E-mail address: smartlabindia@gmail.com.

Abstract. Single crystals of bismaleato lead(IV) [$Pb_2(C_4H_2O_4)_2$] are grown by the controlled diffusion of lead ions in gelated hydrosilica matrix impregnated with maleate ions. The various functional groups present in the compound is identified using FTIR spectrum. The structure of the crystal was elucidated using single crystal XRD studies. It crystallizes in the monoclinic system with space group $P2_1/c$. The TG- DTA analysis was employed l to explore the thermal stability and decomposition the pattern. the dielectric measurements were made over wide frequency and temperature ranges. The optical band gap was determined using diffuse reflectance spectroscopy.

1. Introduction

Metal coordinated dicarboxylates have wide applications in the regimes of ferroelectricity, piezoelectricity, photoconductivity and optical nonlinearity [1-7]. Among dicarboxylates, metal complexes of maleic acid have displayed optical, magnetic and electrical properties [8-10]. A detailed report only on the structural characterization of a lead maleate complex grown by the slow evaporation method [11] is available. As the solubility of metal dicarboxylates is very low in pure water, it is not so easy to grow a them by the slow cooling or slow evaporation methods. Strain free single crystals of good optical quality can be grown by the controlled diffusion technique in inert hydrosilica gel medium and employing this method we have succeeded in growing good crystals of a few maleates [12-15]. Here we present a concise report on the structural, thermal, dielectric and optical properties of lead maleate crystals grown by the above technique.

2. Experimental

Lead maleate crystals were grown in gel matrices taken in straight tubes by titrating maleic acid against sodium meta silicate solutions of different densities (1.03-1.07 g/cc, in steps of 0.01) and pH varying from 4 to 7 [16]. Concentration of the maleic acid was also varied. After ensuring firm gel setting, supernatant solution, lead nitrate, of different molarities (0.25 – 1M) were poured. The tubes were then hermitically sealed and kept undisturbed at room temperature.

The powdered sample was subjected to FTIR Spectroscopic investigations using a Thermo Nicolet Avtar 370 model FTIR Spectrophotometer, in the range 400-4000 cm^{-1} at a resolution of 4 cm^{-1}, using KBr pellet method. The single crystal X-ray diffraction studies were conducted on a good crystal of size 0.15 x 0.15 x 0.10 mm^3 using Bruker AXS Kappa Apex2 CCD Diffractometer with graphite monochromated Mo-Kα radiation. The software APEX2/SAINT [17] was used for the data collection,

cell refinement and data reduction of the crystal.The crystal structure was solved using SIR92 [18] and was refined using SHELXL-97 [19-20]. The Full-matrix least squares refinement based on 931 reflections and 83 parameters along with 48 restraints, converged the residuals to R_1= 0.0490, wR_2= 0.1464. The thermal behaviour of the sample was explored by the Perkin Elmer made Pyris Diamond TG–DTA analyzer. For this the powdered sample was heated from 50 °C to 1030 °C at the rate of 20 °C/min. The dielectric properties of the grown crystal was carried out for wide frequency and temperature ranges using Hioki 3532-50 Hi tester. For this pellets were prepared by the application of 4 tonnes pressure for two minutes. The DRS analysis of the powdered sample was conducted using Jasco UV-Vis-NIR spectrophotometer in the range 200 to 2000 nm.

3. Results and discussion

3.1. Crystal Formation

Optically transparent single crystals with flat surfaces formed within the gel in a period of about 8 weeks. Excellent crystals developed in a gel of density 1.06 gm/cc with 0.75 M concentration of inner maleic acid at pH 6. The outer supernatant lead nitrate solution of strength 0.25 M was poured gently on the set gel. Crystals of dimensions up to 2 x 1 x 1 mm^3 were obtained (Figure 1).

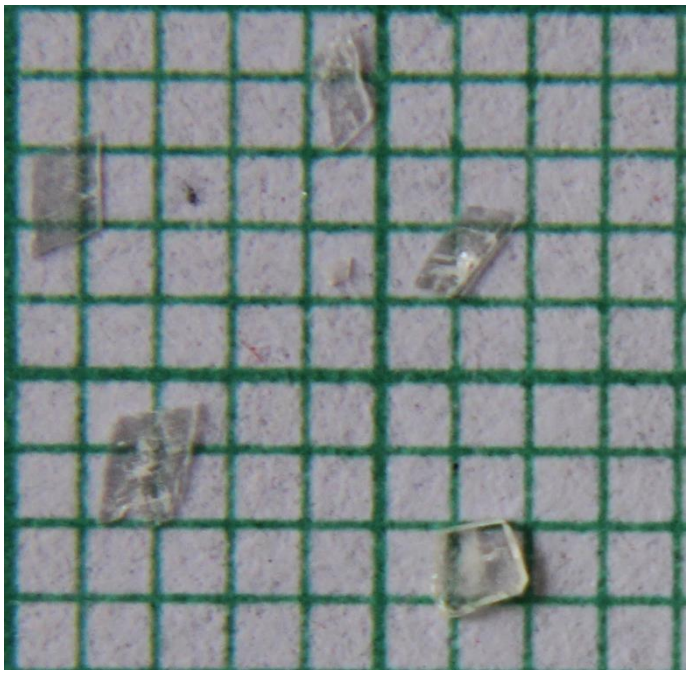

Figure 1. Photographs of the grown crystals.

3.2. FTIR Spectral Analysis

The recorded FTIR spectrum of the sample (Figure 2) is interpreted in the light of the established data of similar compounds [21-23] and found to bear the signatures of all the functional groups in the compound. The stretching mode of the C-H group is depicted with the band at 3008 cm^{-1}. The stretching of the covalent bond C=O is revealed by the peak at 1719 cm^{-1} and its asymmetric stretching is shown by the band at 1672 cm^{-1}. Asymmetric and symmetric stretching of the carboxylate groups occur at wave numbers 1534 cm^{-1} and 1382 cm^{-1} in order. The peaks at 1408 cm^{-1} and at 1303 cm^{-1} represents the deformation of C-H group. The peaks at 1495 cm^{-1}, 1174 cm^{-1} and 905 cm^{-1} is credited to the asymmetric and symmetric stretching of the CC bond. Rocking, twisting and vibration modes of the C-H group happen at 973 cm^{-1}, 834 cm^{-1} and 741 cm^{-1} in order. The metal oxygen stretching

and its combination along with C-C stretching give rise to the respective vibrations at 696 cm^{-1} and 542 cm^{-1}. Vibration mode of the carboxylate group is assigned with the peak at 615 cm^{-1}.

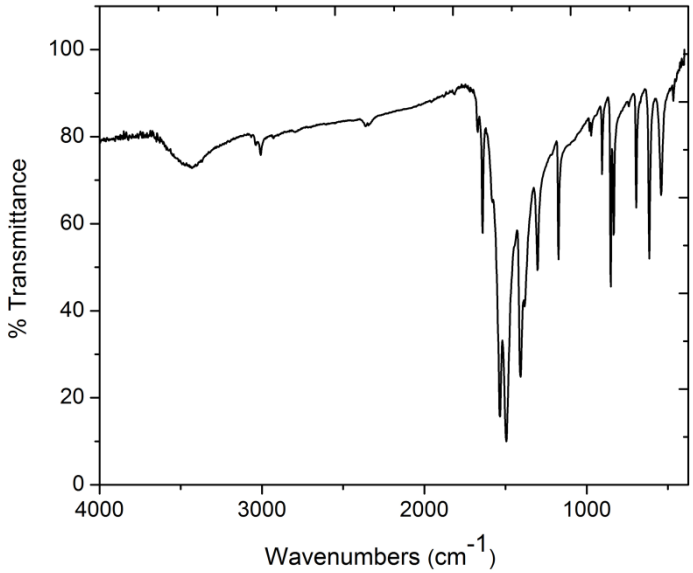

Figure 2. FTIR spectrum of lead maleate.

Table 1. Spectral assignment of IR peaks.

Wave number (cm^{-1})	*Assignment*	*Wave number (cm^{-1})*	*Assignment*
3008	υ C-H	1174	υ_{as} C=C
1719	υ C=O	973	ρ_r C-H
1672	υ_{as} C=O	905	υ_s C=C
1534	υ_{as} COO	834	ρ_t C-H
1495	υ_{as} C=C	741	π C-H
1408	δ C-H	696	υ M-O
1382	υ_s COO	615	π COO
1303	δ C-H	542	υ M-O + υ C-C

3.3. Crystal Structure Analysis

The single crystal X-ray diffraction studies reveal that the crystallized complex is bismaleatolead(IV) $[Pb_2(C_4H_2O_4)_2]$. It crystallizes in the monoclinic system with space group $P2_1/c$ and unit cell dimensions a = 9.8778(13) Å, b = 6.9501(9) Å, c = 8.2630(11) Å, $\alpha = \gamma = 90$ ° and β =111.191(7) °. This matches well the reported structural data [11]. The crystal structure and refinement is displayed in Table 2. The bond lengths and bond angles are listed in Tables 3 and 4. The ORTEP [24-26] of the molecule with thermal ellipsoids at 50% probability is shown in figure 3. The structure of the molecule reveals that each maleate anion acts as tetradendate ligand - bidendate through the oxygen atoms (O1 and O3) of the two carboxylate groups to one Pb^{2+} ion (Pb1) and two monodendate coordination by the other two oxygen atoms (O2 and O4) to adjacent Pb^{2+} ions (Pb2 and Pb3). Thus the compound gets chelated and heightens the thermodynamic stability. The intermolecular hydrogen bonds also increase the stability of the structure. The packing diagram shows that (Figure 4) each Pb^{2+} ion is heptacoordinated to oxygen atoms forming a stable distorted octahedron. Also each Pb^{2+} ion is found to be bonded with two maleate anions.

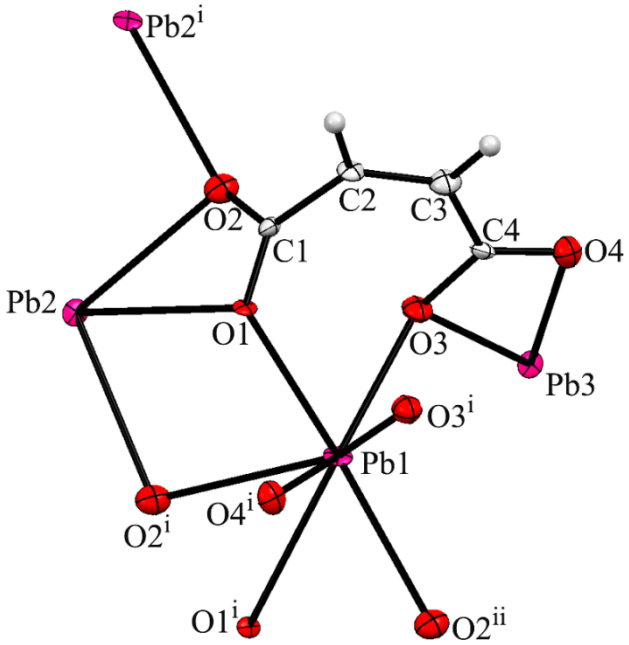

Figure 3. ORTEP of the molecule with 50 % probability.

Table 2. Crystal data and structure refinement.

Empirical formula	$C_8 H_4 O_8 Pb_2$
Formula weight	642.49
Temperature	293(2) K
Wavelength	0.71073 Å
Crystal system, space group	Monoclinic, $P2_1/c$
Unit cell dimensions	a = 9.8778(13) Å, α = 90 ˚ b = 6.9501(9) Å, β = 111.191(7) ˚ c = 8.2630(11) Å, γ = 90 ˚
Volume	528.91(12) Å^3
Z, Calculated density	2, 4.304 Mg/m^3
Absorption coefficient	31.822 mm^{-1}
F(000)	560
Crystal size	0.15 mm x 0.15 mm x 0.10 mm
θ range for data collection	2.21 ˚ to 25 ˚
Limiting indices	-11≤ h ≤11, -7 ≤k ≤8, -7≤ l≤9
Reflections collected / unique	4087 / 931 [R(int) = 0.0647]
Completeness to θ = 25.00 ˚	100.0 %
Absorption correction	Semi-empirical from equivalents
Max. and min. transmission	0.1865 and 0.0845
Refinement method	Full-matrix least-squares on F^2
Data / restraints / parameters	931 / 48 / 83
Goodness-of-fit on F^2	1.120
Final R indices [I>2σ(I)]	R_1 = 0.0490, wR_2 = 0.1464
R indices (all data)	R_1 = 0.0527, wR_2 = 0.1494
Extinction coefficient	0.0031(9)
Largest diff. peak and hole	3.728 and -3.235eÅ^{-3}

Table 3. Bond lengths in bismaleatolead (IV).

Bond	Lengths (Å)	Bond	Lengths (Å)
C(1)-O(2)	1.26(2)	O(1)-Pb(1)#2	2.708(10)
C(1)-O(1)	1.257(19)	O(2)-Pb(1)#2	2.622(12)
C(1)-C(2)	1.46(2)	O(3)-Pb(1)#1	2.422(11)
C(2)-C(3)	1.32(2)	O(3)-Pb(1)	2.660(11)
C(2)-H(2)	0.9300	O(4)-Pb(1)#1	2.523(12)
C(3)-C(4)	1.48(2)	Pb(1)-O(3)#3	2.422(11)
C(3)-H(3)	0.9300	Pb(1)-O(4)#3	2.523(12)
C(4)-O(4)	1.204(19)	Pb(1)-O(2)#4	2.622(12)
C(4)-O(3)	1.318(18)	Pb(1)-O(1)#4	2.708(10)
C(4)-Pb(1)#1	2.814(16)	Pb(1)-C(4)#3	2.814(16)
O(1)-Pb(1)	2.432(10)		

Table 4. Bond angles of bismaleatolead(IV).

Bond	Angles (°)	Bond	Angles (°)
O(2)-C(1)-O(1)	121.6(14)	C(4)-O(4)-Pb(1)#1	90.9(9)
O(2)-C(1)-C(2)	117.7(14)	O(3)#3-Pb(1)-O(1)	81.4(4)
O(1)-C(1)-C(2)	120.5(14)	O(3)#3-Pb(1)-O(4)#3	53.1(4)
C(3)-C(2)-C(1)	126.9(15)	O(1)-Pb(1)-O(4)#3	80.5(3)
C(3)-C(2)-H(2)	116.6	O(3)#3-Pb(1)-O(2)#4	72.8(4)
C(1)-C(2)-H(2)	116.6	O(1)-Pb(1)-O(2)#4	73.0(4)
C(2)-C(3)-C(4)	123.4(14)	O(4)#3-Pb(1)-O(2)#4	122.5(4)
C(2)-C(3)-H(3)	118.3	O(3)#3-Pb(1)-O(3)	142.2(4)
C(4)-C(3)-H(3)	118.3	O(1)-Pb(1)-O(3)	70.6(3)
O(4)-C(4)-O(3)	122.4(14)	O(4)#3-Pb(1)-O(3)	96.5(3)
O(4)-C(4)-C(3)	121.8(13)	O(2)#4-Pb(1)-O(3)	119.8(4)
O(3)-C(4)-C(3)	115.8(13)	O(3)#3-Pb(1)-O(1)#4	79.8(3)
O(4)-C(4)-Pb(1)#1	63.7(9)	O(1)-Pb(1)-O(1)#4	121.5(2)
O(3)-C(4)-Pb(1)#1	59.3(8)	O(4)#3-Pb(1)-O(1)#4	125.6(3)
C(3)-C(4)-Pb(1)#1	169.7(10)	O(2)#4-Pb(1)-O(1)#4	48.6(4)
C(1)-O(1)-Pb(1)	121.7(9)	O(3)-Pb(1)-O(1)#4	136.6(3)
C(1)-O(1)-Pb(1)#2	92.6(8)	O(3)#3-Pb(1)-C(4)#3	27.9(4)
Pb(1)-O(1)-Pb(1)#2	110.0(4)	O(1)-Pb(1)-C(4)#3	82.0(4)
C(1)-O(2)-Pb(1)#2	96.7(9)	O(4)#3-Pb(1)-C(4)#3	25.3(4)
C(4)-O(3)-Pb(1)#1	92.8(9)	O(2)#4-Pb(1)-C(4)#3	99.7(4)
C(4)-O(3)-Pb(1)	121.4(9)	O(3)-Pb(1)-C(4)#3	120.2(4)
Pb(1)#1-O(3)-Pb(1)	112.7(4)	O(1)#4-Pb(1)-C(4)#3	103.1(4)

Symmetry transformations used to generate equivalent atoms:
#1 x,-y+1/2,z-1/2 #2 -x+1,y+1/2,-z+1/2
#3 x,-y+1/2,z+1/2 #4 -x+1,y-1/2,-z+1/2

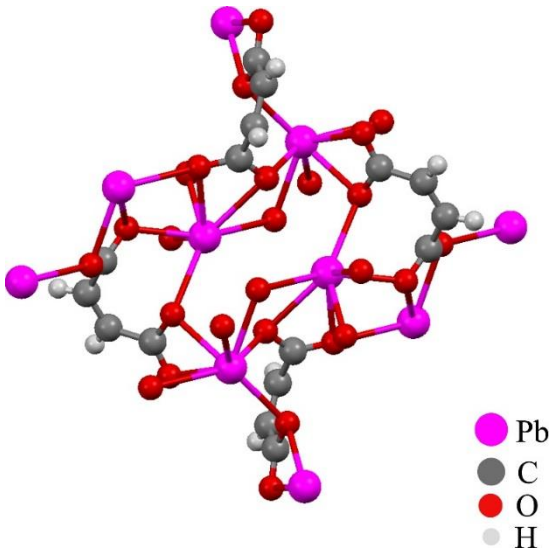

Figure 4. Polymeric structure of lead maleate

3.4. Thermal Studies

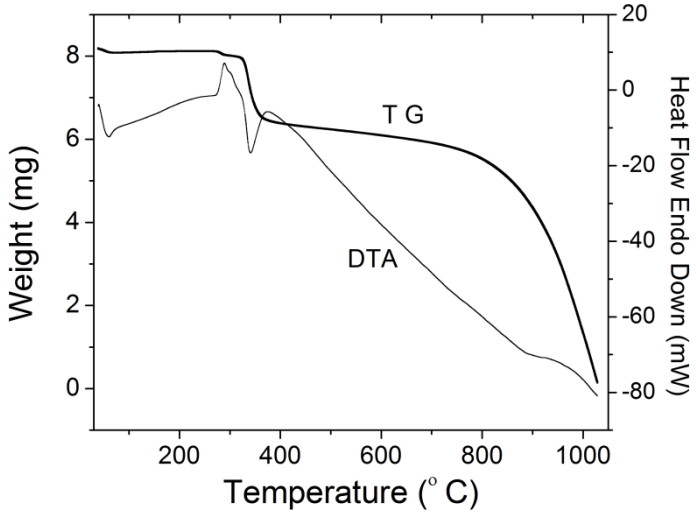

Figure 5. TG- DTA curves of bismaleatolead(IV).

The analysis of the TG-DTA curves (Figure 5) reveals the thermal stability and decomposition pattern of the grown sample. The TG curve indicates that the material is thermally stable up to 274 °C. It is also to be noted that the TG curve does not show any considerable weight loss till this temperature. Upon heating the sample to 338 °C, the compound turns to lead oxalate by the removal of acetylene molecules. The exothermic peak at 289 °C in DTA confirms this decomposition. During the next stage of heating to 355 °C, expulsion of carbon monoxide takes place leaving behind lead carbonate. The broad exothermic peak which starts immediately after 340 °C in the DTA is indicative of this stage. Further heating the material up to 799 °C, it gets transformed into lead oxide by the elimination of carbon dioxide molecules. This transformation is shown in the DTA by the endothermic peak which starts beyond 378 °C. The agreement between the observed and calculated mass loss matches well in each stage and is given in Table 5. The TG curves also displays that the weight loss continues even after 1000 °C, which may be due to reduction of lead oxide to the stable metallic lead.

The stoichiometry of the crystallized complex is evident from the thermal studies also and hence the chemical reaction leading to the formation of the title compound is:

$$2\ Pb(NO_3)_2 + 2\ C_4H_4O_4 \rightarrow Pb_2(C_4H_2O_4)_2 + 4\ HNO_3.$$

Table 5. The decomposition process of $Pb_2(C_4H_2O_4)_2$.

Stage	Decomposition temperature(°C)	Product after decomposition	Molecules evolved	Observed mass loss(%)	Calculated mass loss(%)
1	274-338	$Pb_2(C_2O_4)_2$	$2C_2H_2$	8.193	8.104
2	338-355	$Pb_2(CO_3)_2$	2CO	8.844	8.719
3	355-799	2PbO	$2CO_2$	14.207	13.699

3.5. Dielectric Studies

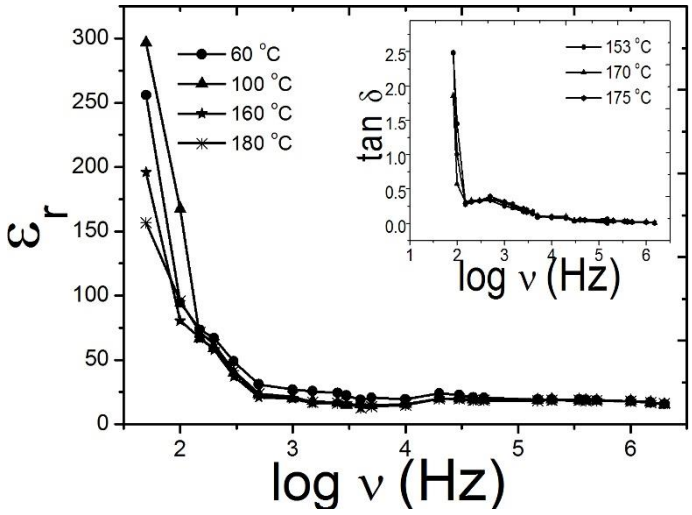

Figure 6. Frequency response of dielectric constant and dielectric loss.

Figure 6 shows that the value of dielectric constant and loss tangent is greater at low frequencies. The higher value of dielectric constant at low frequencies is mainly due to the presence of interfacial polarization and that of loss tangent is attributed to the space charge polarization [27-28]. The dielectric constant decreases with increasing frequency, depending on the fact that beyond certain frequency of the electric field, the dipole does not follow the applied alternating field [29-30]. The low dielectric loss at high frequency ensures that the grown crystals are of good optical quality.

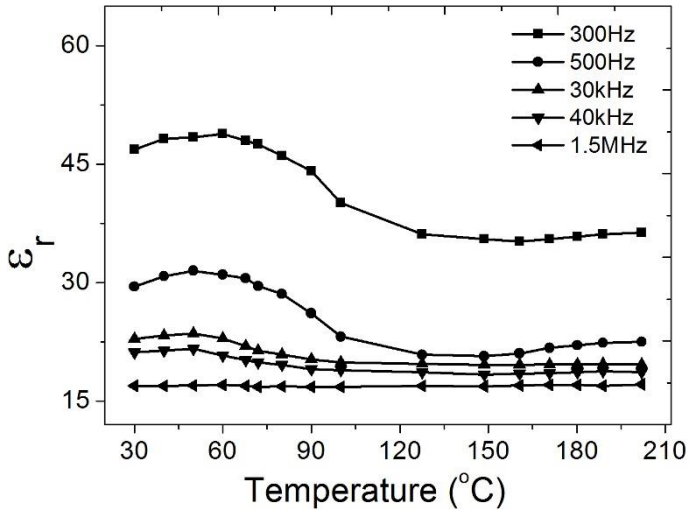

Figure 7. Thermal response of dielectric constant.

The variation of the dielectric constant and loss with temperature is depicted in figure 7. The slightly higher dielectric permittivity for low frequencies confirms the presence of interfacial polarization in the material. The dielectric constant displays a slight increase near 60 °C only at lower frequencies and for higher frequencies (40 kHz and 1.5 MHz), the dielectric constant is almost temperature independent, indicating the good chemical homogeneity [31] and structural stability of the grown crystals.
The ac conductivity of the material is estimated using the relation $\sigma_{ac} = \acute{\varepsilon}\ \varepsilon_0\ \omega\tan\delta$ and it shows almost similar behaviour both for high and low frequencies (Figure 8). It can also be seen that the conductivity displays usual behaviour of maleates with slightly elevated value for high frequencies and almost temperature independent behaviour.

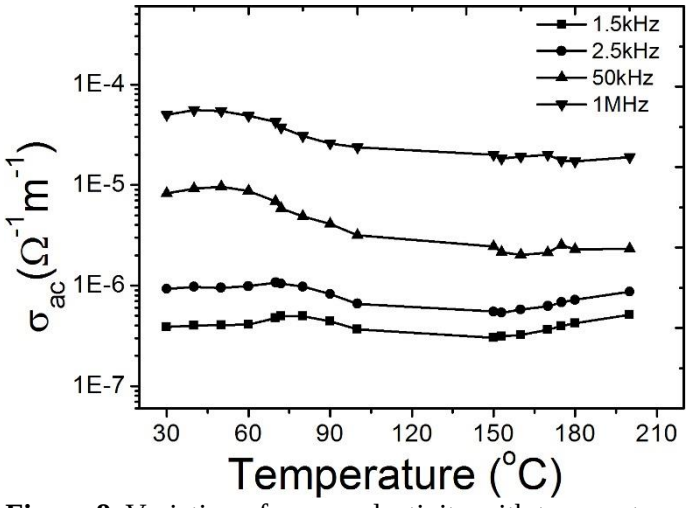

Figure 8. Variation of a.c. conductivity with temperature.

3.6. Diffuse Reflectance Spectroscopy

The diffuse reflectance spectrum of the title compound in the UV-Vis-NIR region is shown in figure 9. The band gap is determined using the Kubelka Munk Theory [32-33]. The Kubelka–Munk remission function F(R) at each wavelength λ is given by $F(R) = (1-R)^2/2R = k/s$, R being the reflectance of the sample, k is the absorption coefficient and s is the scattering coefficient.

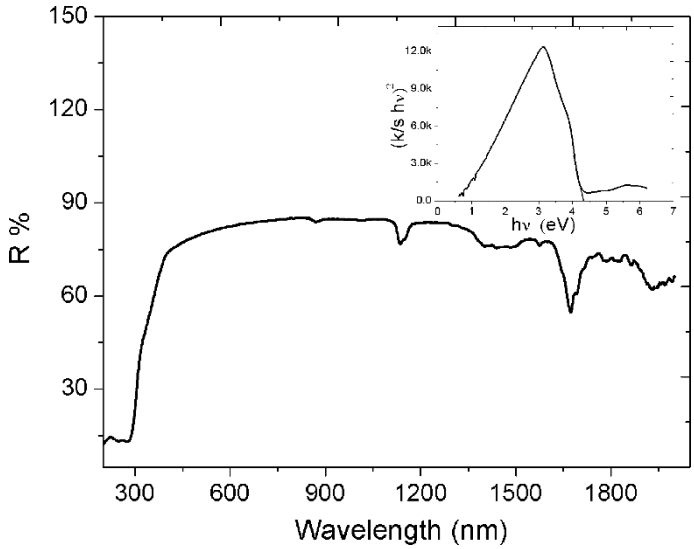

Figure 9. Diffuse reflectance spectrum of the compound.

The plot of $((k/s)hv)^2$ versus hv (inset of figure 9) was drawn and the optical band gap (E_g) is evaluated from the linear fit of the curve on the energy axis is 4.32 eV.

4. Conclusions

Well faceted, transparent single crystals of bismaleato lead have been developed by the controlled diffusion of aqueous solutions of maleic acid and lead nitrate in silica gel. The functional groups were determined from FTIR spectroscopy. The single XRD studies revealed that the complex crystallized in the monoclinic system with space group $P2_1/c$ with unit cell dimensions $a = 9.8778(13)$ Å, $b = 6.9501(9)$ Å, $c = 8.2630(11)$ Å, $\alpha = \gamma = 90$ ° and $\beta = 111.191(7)$ °. The TG-DTA analyses showed that the compound is thermally stable up to 274 °C. The dielectric and ac conductivity studies show that the compound exhibits normal dielectric behavior. The optical band gap of the material explored using the DRS studies is 4.32 eV.

5. References

[1] Dalal P V and Saraf K B 2006 *Bull. Mater. Sci.* **29** 421
[2] Arora S K, Patel V, Patel R G, Amin B and Kothari A 2004 *J. Phys. Chem. Solids* **65** 965
[3] Jini T, Saban K V and Varghese G 2006 *Cryst. Res. Technol.* **41** 250
[4] Jini T, Saban K V, Varghese G, Naveen S, Sridhar M A and Prasad J S 2007 *J. Alloys Compd.* **433** 211
[5] Lincy A, Mahalakshmi V, Tinto A J, Thomas J and Saban K V 2010 *Physica B* **405** 4673
[6] Doreswamy B H, Mahendra M, Sridhar M A, Prasad J S, Varughese P A, George J and Varghese G 2005 *Mater. Lett.* **59** 1206
[7] Varghese M, Lizymol X, Mahadevan C K and Abraham K E 2011 *Phys. Scr.* **83** (3) 035801
[8] Bharthasarthi T, Arulmozhichelvan P and Murugakoothan P 2010 *Mater. Lett.* **64** 1506
[9] Natarajan S, Britto S A M and Ramachandran E 2006 *Cryst. Growth Des.* **6** (1) 137
[10] Oczko G, Legendziewicz J, Wickleder M S and Meyer G 2002 *J. Alloys Compd.* **341** 255
[11] Bonhomme F et al. 2005 *Inorg Chem.* **44** 7394
[12] Mahalakshmi V, Lincy A, Thomas J and Saban K V 2012 *J. Phys. Chem. Solids* **73** 584
[13] Mahalakshmi V, Lincy A, Thomas J and Saban K V 2013 *IOSR J. Appl. Phys.* **4** 67
[14] Mahalakshmi V, Lincy A, Thomas J and Saban K V 2014 *Optik – Int. J. Light Electron Opt.* **125** 191
[15] Mahalakshmi V, Lincy A, Thomas J and Saban K V 2015 *Optik – Int. J. Light Electron Opt.* **126** 2419
[16] Henisch H K 1970 *Crystal growth in Gels* (Pittsburg: Pennsylvania University Press) p 20
[17] Bruker 2004 *APEX2, SAINT and XPREP* Bruker AXS Inc. Madison, Wisconsin, USA
[18] Altomare A, Cascarano G, Giacovazzo C and Guagliardi A 1993 *J. Appl. Crystallogr.* **26** 343
[19] Sheldrick G M 1997 SHELXL-97 *Program for the Refinement of Crystal Structures* Germany: University of Göttingen
[20] Sheldrick G M 2008 *Acta Cryst.* A **64** 112
[21] Bellamy L J 1975 *The IR Spectra of Complex Molecules* vol 1 (London: Chapman and Hall) 3rd ed
[22] Nakamoto K 1963 *Infrared Spectra of Inorganic and Coordination Compounds* part III (New York: John Wiley and sons) 6th ed p 62
[23] Edsall J T 1937 *J. Chem. Phys.* **5** 508
[24] Spek A L 1990 *Acta Cryst.* A **46** C34
[25] Spek A L 1998 *PLATON* A Multipurpose Crystallographic Tool (The Netherlands: University of Utretcht)
[26] Farrugia L J 1997 *J. Appl. Cryst.* **30** 565
[27] Boaz B M, Selvaraj R S, Kumar K S and Das S J 2009 *Indian J. Phys.* **83** (12) 1647
[28] Raj C J, Krishnan S, Dinakaran S, Linet J M, Uthrakumar R, Robert R and Das S J 2009 *J. Mater. Sci. Technol.* **25** 745
[29] Sharma K K, Kotru P N, Tandon R P and Wanklyn B M 1998 *J. Phys. Cond. Matt.* **10** 5277
[30] Mazen S A, Metawe F and Mansour S F 1997 *J. Phys. D: Appl. Phys.* **30** 1799
[31] Babu G A, Sreedhar S, Rao S V and Ramasamy P 2010 *J. Cryst. Growth* **312** 1957
[32] Kubelka P and Munk F 1931 *Z. Tech. Phys.* (Leipzig) **12** 593

[33] Kubelka P 1948 *J. Opt. Soc. Am.* **38** 448